
Biodistribution and Dosimetry of Intraventricularly Administered ^{124}I -Omburtamab in Patients with Metastatic Leptomeningeal Tumors

Neeta Pandit-Taskar^{1,2}, Pat B. Zanzonico^{1,3}, Kim Kramer⁴, Milan Grkovski³, Edward K. Fung³, Weiji Shi⁵, Zhigang Zhang⁵, Serge K. Lyashchenko⁶, Alex M. Fung¹, Keith S. Pentlow³, Jorge A. Carrasquillo¹, Jason S. Lewis^{1,2,6}, Steven M. Larson^{1,7}, Nai-Kong V. Cheung⁴, and John L. Humm^{1,3}

¹Department of Radiology, Memorial Sloan Kettering Cancer Center, New York, New York; ²Department of Radiology, Weill Cornell Medical College, New York, New York; ³Department of Medical Physics, Memorial Sloan Kettering Cancer Center, New York, New York; ⁴Department of Pediatrics, Memorial Sloan Kettering Cancer Center, New York, New York; ⁵Department of Biostatistics and Epidemiology, Memorial Sloan Kettering Cancer Center, New York, New York; ⁶Radiochemistry and Molecular Imaging Probe Core, Memorial Sloan Kettering Cancer Center, New York, New York; and ⁷Molecular Pharmacology Program, Memorial Sloan Kettering Cancer Center, New York, New York

Radiation dose estimations are key for optimizing therapies. We studied the role of ^{124}I -omburtamab (8H9) given intraventricularly in assessing the distribution and radiation doses before ^{131}I -omburtamab therapy in patients with metastatic leptomeningeal disease and compared it with the estimates from cerebrospinal fluid (CSF) sampling. **Methods:** Patients with histologically proven malignancy and metastatic disease to the central nervous system or leptomeninges who met eligibility criteria for ^{131}I -omburtamab therapy underwent immuno-PET imaging with ^{124}I -8H9 followed by ^{131}I -8H9 antibody therapy. Patients were imaged with approximately 74 MBq of intraventricular ^{124}I -omburtamab via an Ommaya reservoir. Whole-body PET images were acquired at approximately 4, 24, and 48 h after administration and analyzed for dosimetry calculations. Peripheral blood and CSF samples were obtained at multiple time points for dosimetry estimation. **Results:** Forty-two patients with complete dosimetry and therapy data were analyzed. ^{124}I -omburtamab PET-based radiation dosimetry estimations revealed mean (\pm SD) absorbed dose to the CSF for ^{131}I -8H9 of 0.62 ± 0.40 cGy/MBq, compared with 2.22 ± 2.19 cGy/MBq based on ^{124}I -omburtamab CSF samples and 1.53 ± 1.37 cGy/MBq based on ^{131}I -omburtamab CSF samples. The mean absorbed dose to the blood was 0.051 ± 0.11 cGy/MBq for ^{124}I -omburtamab samples and 0.07 ± 0.04 cGy/MBq for ^{131}I -omburtamab samples. The effective whole-body radiation dose for ^{124}I -omburtamab was 0.49 ± 0.27 mSv/MBq. The mean whole-body clearance half-time was 44.98 ± 16.29 h. **Conclusion:** PET imaging with ^{124}I -omburtamab antibody administered intraventricularly allows for noninvasive estimation of dose to CSF and normal organs. High CSF-to-blood absorbed-dose ratios are noted, allowing for an improved therapeutic index to leptomeningeal disease and reduced systemic doses. PET imaging-based estimates were less variable and more reliable than CSF sample-based dosimetry.

Key Words: ^{124}I ; PET; radioimmunotherapy; cerebrospinal fluid; intraventricular

J Nucl Med 2019; 60:1794–1801

DOI: 10.2967/jnumed.118.219576

Central nervous system metastasis is seen in advanced stages of several pediatric and adult malignancies, including leukemia, neuroblastoma, medulloblastoma, and other solid tumors, and is associated with significant morbidity and high mortality. For patients with high-risk neuroblastoma, the incidence of metastatic disease to the central nervous system and of recurrence is increasing (1,2). The cerebrospinal fluid (CSF) space is believed to be a conduit for leptomeningeal spread and a site for metastasis. Intrathecal or intracavitary administration of radiolabeled antibodies has been successfully applied in other malignancies, such as malignant gliomas, with low toxicity and encouraging results (3,4). We have previously reported on the use of radioimmunotherapy (5) and the feasibility of intrathecal therapy with monoclonal antibodies (2,6,7) in neuroblastoma. We have used single-photon imaging with the ^{131}I -labeled antibody 3F8, which targets disialoganglioside 2-expressing tumors, for imaging and dosimetry estimations (6,7). A murine monoclonal antibody, omburtamab (8H9), targets the glycoprotein B7-H3 on cell membranes and is expressed in several human solid tumors, including neuroblastoma (8,9). We evaluated pretherapy PET imaging with intraventricular injection for estimating radiation doses to CSF in patients with known leptomeningeal disease undergoing treatment with ^{131}I -omburtamab and compared the PET-based dose estimates with those from CSF sampling.

MATERIALS AND METHODS

This prospective study of ^{124}I -omburtamab and ^{131}I -omburtamab imaging and therapy was performed under an institutional review board-approved (Clinicaltrials.gov NCT00089245) and a U.S. Food and Drug Administration-approved Investigational New Drug application (BB-IND 9351). All patients or their legal guardians provided written informed consent.

Received Aug. 23, 2018; revision accepted May 2, 2019.
For correspondence or reprints contact: Neeta Pandit-Taskar, Molecular Imaging and Therapy Service, Department of Radiology, Memorial Sloan Kettering Cancer Center, 1275 York Ave., New York, NY 10065.
E-mail: pandit-n@mskcc.org
Published online Aug. 12, 2019.
COPYRIGHT © 2019 by the Society of Nuclear Medicine and Molecular Imaging.

TABLE 1
Patient Demographics

Demographic	Data
Total number of patients	42
1 dose	20
2 doses	22
Primary malignancy	
Neuroblastoma	32
Medulloblastoma	2
Sarcoma	3
Ependymoma	1
Rhabdoid tumor	1
Melanoma	1
Chordoma	1
Choroid plexus tumor	1
Age range	3 mo–42 y
Sex	
Male	26
Female	16

Data are *n*, except for age.

Patients with histologically confirmed diagnosis of a malignancy with omburtamab reactivity and with evidence of central nervous system or leptomeningeal disease who met all other eligibility criteria for therapy with intraventricular ¹³¹I-omburtamab were studied. The characteristics of the study population are presented in Table 1; the study schema is shown in Figure 1. Patients with obstructive or symptomatic communicating hydrocephalus and those who had received cranial or spinal irradiation less than 3 wk before the start of the protocol were excluded. All patients underwent a CSF flow study with ¹¹¹In-DTPA imaging to ensure patency of the Ommaya reservoir and adequate CSF flow. Patients underwent a pretherapy dosimetry study with ¹²⁴I-omburtamab PET imaging, which was used to estimate absorbed radiation dose to the CSF and normal organs. Subsequently, patients were treated with ¹³¹I-omburtamab within 1 wk at various therapeutic dose levels, as detailed below. Multiple CSF and blood samples were obtained after ¹²⁴I-omburtamab administration and after therapy with ¹³¹I-omburtamab to estimate the radiation dose to CSF and blood. Predicted dosimetry from ¹²⁴I-omburtamab and the actual therapeutic ¹³¹I-omburtamab dosimetry were compared.

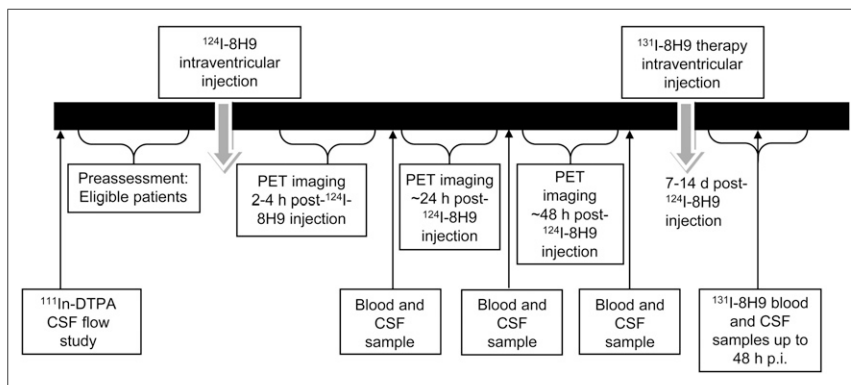


FIGURE 1. Study schema.

¹²⁴I-Omburtamab Radiolabeling

Radiolabeling of ¹²⁴I-omburtamab was performed by the Radiochemistry and Molecular Imaging Probes core facility. ¹²⁴I-omburtamab was prepared using approximately 1 mg of the unlabeled antibody and up to 1,295 MBq (35 mCi) of ¹²⁴I (produced by the institutional core facility) with the Iodo-Gen (Pierce Biotechnology, Inc.) method, followed by purification with an anion exchange resin and terminal sterilization by microfiltration. Before the release for patient administration, the ¹²⁴I-omburtamab drug product was tested to ensure radiochemical purity of at least 90%, as determined by thin-layer radiochromatography and immunoreactive fraction determination using a live antigen-expressing cell assay. Sterility testing by medium inoculation was performed after release. Final prepared patient-specific unit doses comprised 74 MBq (2.0 mCi) of ¹²⁴I-omburtamab, containing 1.0 mg of the monoclonal antibody, formulated in approximately 0.8–2.2 mL of approximately 3%–5% (v/v) human serum albumin solution in phosphate buffer. The therapeutic antibody's specific activity was 1,295–1,850 MBq/mg (35–50 mCi/mg).

Administration

Patients were prepared with liothyronine sodium (Cytomel; Jones Medical Industries) and saturated solution of potassium iodide for thyroid protection before infusion of both the ¹²⁴I dosimetry and the ¹³¹I therapeutic administrations. Both imaging and treatment dose were given via the Ommaya shunt, accessed using sterile precautions. A baseline CSF sample was drawn for pharmacokinetic analysis (1–2 mL) followed by an additional 2–3 mL of CSF for flush. After confirmation of a good CSF flow return, the radiolabeled ¹²⁴I-omburtamab was injected slowly over approximately 1 min followed by 1% human serum albumin (~1 mL) and CSF flush (total volume ≤ 3 mL). The therapeutic dose of ¹³¹I-omburtamab was administered via the Ommaya shunt using the same technique within a week of the imaging study.

Imaging

Three PET scans were performed at approximately 4, 24, and 48 h after ¹²⁴I-omburtamab injection. All scans were performed from vertex to pelvis, in 2-dimensional mode on a GE Healthcare Discovery PET/CT scanner, using the ¹²⁴I setting (positron yield, 0.23; physical half-life, 4.18 d) and a duration of 4 min per field of view on the day of the radiolabeled antibody administration and 5 min on subsequent imaging days. PET emission data were corrected for attenuation, scatter, and random events and reconstructed into a 128 × 128 × 47 matrix (voxel dimensions, 5.47 × 5.47 × 3.27 mm) using the GE ordered-subset expectation maximization algorithm with standard clinical reconstruction parameters: 2 iterations, 16 subsets, and a gaussian postprocessing filter with a full width at half maximum of 6.0 mm. Since all PET acquisitions were conducted in 2-dimensional mode, no specialized reconstruction software was required to account for prompt ¹²⁴I γ-ray emissions.

PET Scan-Based Dosimetry

Volumes of interest (VOIs) were generated over liver, salivary glands, spleen, stomach contents, thyroid, and brain for each of the 3 time-point images using Hermes Hybrid Viewer (Hermes Medical Solutions). Whole-body counts were obtained from scanner acquisition data. The VOIs encompassing the entire CSF pool in the spinal canal, as well as the CSF subvolumes in lateral ventricles and cervical, thoracic, and lumbar spine, were created. CSF and organ time-activity concentration curves were fit to exponential functions, and values were decay-corrected for ¹²⁴I. Areas under the concentration curves were determined by analytic integration to infinity of

the fitted exponential functions, incorporating the physical decay of the therapeutic radionuclide ^{131}I to yield the cumulated activity concentrations per unit administered activity of ^{131}I in the CSF and organs. Whole-organ cumulated activities per unit administered activity of ^{131}I were then calculated by multiplying the organ areas under the concentration curves by the corresponding reference organ masses (Oak Ridge National Laboratory) linearly scaled to the respective patient's whole-body mass and used to estimate mean organ-absorbed doses using the OLINDA/EXM software (10).

The narrow cylindrical shape and diameters (average, 13–15 mm) of the spinal column containing the CSF resulted in an unknown partial-volume error (11,12). Doses were estimated to the entire CSF and 4 subregions (lateral ventricles and cervical, thoracic, and lumbar spine), based on the maximum activity concentration (MBq/mL, equivalent to MBq/g assuming unit-density tissue) for each VOI. This was done to investigate possible differences along the length of the spinal column resulting from small occult-disease plaques on the leptomeninges.

The PET data for all regions were fit to a single exponential clearance function, and the curves were integrated to yield a cumulative activity within each of the VOI-defined CSF compartments. On the basis of their respective physical half-lives, the ^{124}I data were converted to the corresponding data for ^{131}I and multiplied by the equilibrium dose constant for ^{131}I for all electron emissions (β , internal conversion, and Auger electrons). We obtained the absorbed doses to the CSF, assuming total local absorption of all electron emissions.

CSF Sample-Based Dosimetry

Multiple CSF samples were obtained via the Ommaya access after ^{124}I -omburtamab dosimetry and ^{131}I -omburtamab therapeutic administrations, including a baseline sample before injection and again at 15 ± 5 , 30 ± 5 , 60 ± 5 , and 120 ± 10 min and at 2–4, 18–24, and 42–48 h after injection. For all samples, an initial 3 mL of CSF were discarded and an additional 1–2 mL were used for assay and counting. Activity in measured CSF aliquots (10 μL) was measured in duplicate using a NaI (Tl) scintillation well counter (Wallac Wizard 1480 automatic γ -counter; Perkin Elmer) together with appropriate standards. The measured count rates were corrected for background count rate and converted to percentage injected activity per gram, decay-corrected to the time of administration. The CSF sample data were fit to a biexponential function. The clearance curve $Y(t)$ was multiplied by the exponential decay factor for the projected therapy radionuclide ^{131}I (physical half-life, 8.02 d). Integration of this function provided the cumulated activity concentration of ^{131}I , which, when multiplied by the equilibrium dose constant for all ^{131}I nonpenetrating emissions (β , internal conversion, and Auger electrons) (0.405 g-cGy/ $\mu\text{Ci}\cdot\text{h}$) (13), yields the mean absorbed dose to the CSF per unit administered activity of ^{131}I in cGy/MBq. This assumes complete local absorption of the β -particles, internal conversion, and Auger electrons and ignores the much lower γ -ray dose contribution.

Blood Measurements

Multiple blood samples were obtained, including a baseline sample before injection of ^{124}I -omburtamab at 15 ± 5 , 30 ± 5 , 60 ± 5 , and 120 ± 10 min and at 2–4, 18–24, and 42–48 h after injection. Samples were counted in duplicates in the LKB Wallac scintillation well counter, calibrated with a ^{124}I standard, and checked for constancy with a ^{68}Ge (271 d) β^+ -emitting standard. The data were subsequently analyzed similarly to the CSF samples.

Statistical Analysis

Statistical analysis was performed to assess whether the radiation doses to the CSF as determined by serial PET VOI analysis were equivalent to those determined from CSF samples. We also examined the ability of ^{124}I -omburtamab imaging to predict the radiation dose for actual therapeutic ^{131}I -omburtamab administrations. The analysis was performed

on paired samples of CSF and blood obtained from tracer and therapy administrations for each patient.

Wilcoxon signed-rank tests were used to detect shifts of median values between paired observations, and Pearson correlation coefficients were calculated to demonstrate correlations between them. To examine the agreement between paired measurements, Bland–Altman plots were generated. To quantitatively assess the agreement, we computed the intraclass correlation coefficient. Statistical software SAS 9.4 (SAS Institute) and R 3.1.1 (<https://www.r-project.org/>) with packages “ICC,” “psych,” and “Bland–Altman Leh” were used for this analysis. All statistical tests were 2-sided, and a P value of less than 0.05 was considered statistically significant.

RESULTS

Patients

Forty-two patients underwent dosimetric imaging with ^{124}I -omburtamab, with 22 patients undergoing a second evaluation of ^{124}I -omburtamab (Table 1). Patients included those with metastatic neuroblastoma ($n = 32$), medulloblastoma ($n = 2$), sarcoma ($n = 3$), and other ($n = 5$), including ependymoma, rhabdoid tumor, melanoma, choroid plexus tumor, and chordoma. The average patient age was 7.5 y (range, 3 mo–42 y), with 26 male and 16 female patients. The mean injected activity of ^{124}I -omburtamab was 71.4 MBq (range, 48.1–77.7 MBq) (1.93 mCi; range, 1.3–2.1 mCi), and specific activity was 74 MBq/mg (2 mCi/mg). Administered ^{131}I -omburtamab activities ranged between 1,258 and 2,960 MBq (34–80 mCi) with specific activity of 1,295–1,850 MBq/mg (35–50 mCi/mg).

Biodistribution on PET Images

All patients received an intraventricular injection of approximately 74 MBq (2 mCi) of ^{124}I -omburtamab via Ommaya catheter. The PET image quality of the study subjects was good despite the low administered activity (37–74 MBq; 1–2 mCi) of the ^{124}I -mAb omburtamab (Fig. 2). The first image acquired between 2 and 4 h after injection showed activity mostly in the ventricles and dispersed in the CSF space along the spinal cord down to the level of the cauda equina by 4 h. Activity distributed in the subarachnoid space along the cerebral convexity was visible at 24 h, with spinal canal activity decreasing by 48 h. PET scans showed variable early distribution in the subarachnoid space and progressive dispersion over the convexity by 24 and 48 h. There was minimal or no activity beyond CSF space and within other organs by 2–4 h after injection. Systemic distribution with visualization of mild activity in other organs was noted by 24 h. This activity increased at 48 h after injection, with low amounts noted in the liver, spleen, kidney, and bladder, as well as minimal thyroid and mild stomach activity noted in some patients (Fig. 2). The uptake in liver showed a slight increase by 48 h. Bladder activity increased with time but remained low because of low systemic activity overall. The thyroid activity decreased by 48 h in most patients. Stomach activity was seen variably, mostly appearing at 24 or 48 h. Activity at the site of injection into Ommaya was always seen; however, the amount varied among patients. This probably affected the CSF clearance and dose calculations.

In 3 patients, prominent activity persisted up to day 2 at the Ommaya reservoir, indicating poor mixing with the flowing CSF compartment; a second, longer, component, consistent with longer biologic clearance from the CSF compartment, was seen in these patients. Clearance of activity from the ventricles based on ^{124}I -omburtamab imaging showed a mean half-life of 9.5 h, ranging up to 18 h in all except 2 patients, one with a clearance half-life of 26 h and another outlier with a substantially high clearance half-life

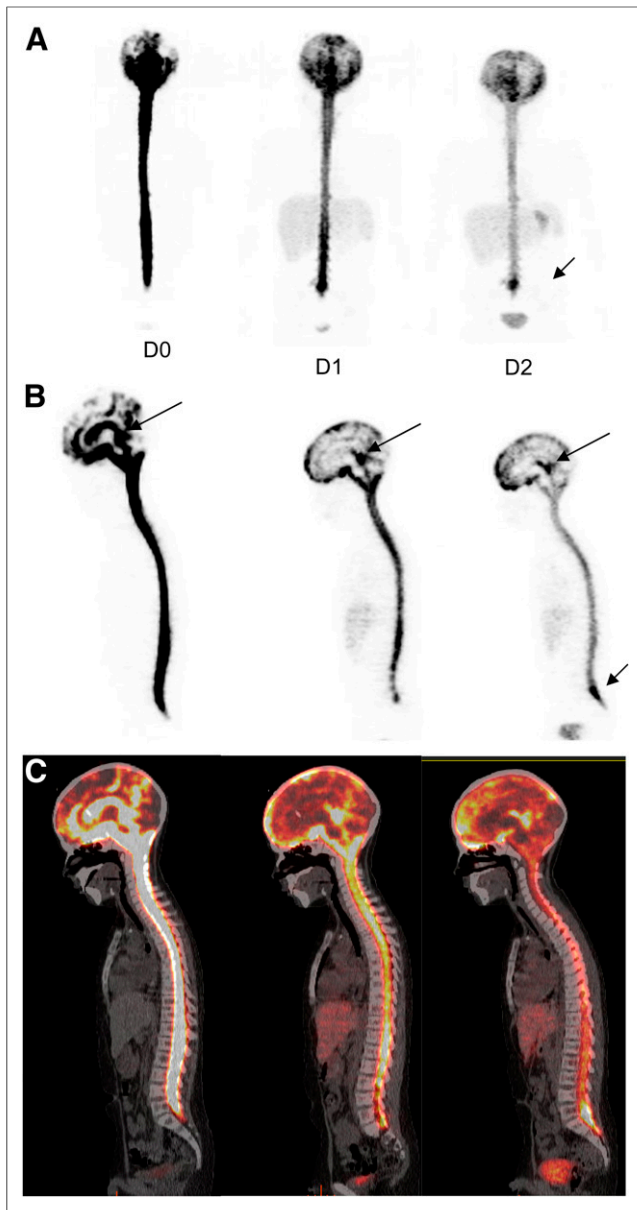


FIGURE 2. Serial ^{124}I -omburtamab images in patient with metastatic neuroblastoma with leptomeningeal disease: anterior maximum-intensity projections (A), sagittal PET projections (B), and fused images (C) from D0, D1, and D2 show activity within ventricles and CSF canal that decreases over time. Systemic activity is seen in liver and bladder in D1 and D2. Clearance from ventricles is slower (long arrows). Pooling is also seen along cauda equina (short arrow).

of 44.4 h (>4 times the average). Mild pooling in the Ommaya or asymmetric activity in the ventricles associated with postsurgical changes and cavities was observed up to 24 h and decreased or resolved by 48 h in 12 patients. In these patients, CSF clearance half-life ranged from 5.5 to 13.8 h for the second component.

Dosimetry Based on ^{124}I -Omburtamab PET

For ^{124}I -omburtamab, mean whole-body clearance half-time was 44.98 ± 16.29 h. The whole-body dose was 0.45 ± 0.27 mGy/MBq, and the effective dose was 0.49 ± 0.27 mSv/MBq. The dosimetry in normal organs (Table 2) showed that the liver received the highest dose, 1.58 ± 1.04 mGy/MBq, followed by normal brain

parenchyma, which received an average dose of 1.13 ± 0.55 mGy/MBq. The radiation dose to thyroid was low, averaging 0.58 mGy/MBq.

The biologic half-lives and dosimetry estimates for these subcompartments derived from PET data are presented in Tables 3 and 4. The average clearance half-time for the entire CSF was 9.85 h. The ^{124}I -mAb-omburtamab dose estimates to CSF in lateral ventricles were 0.620 ± 0.395 cGy/MBq, whereas those for cervical, thoracic, and lumbar regions ranged from 0.445 to 0.567 cGy/MBq. The CSF in ventricles received the highest radiation dose of the other spinal canal areas. However, the mean and median doses to the different subcompartments of the spinal canal did not significantly differ from one another. In 1 patient, the PET estimate was substantially higher than the mean value, attributed to slow clearance from the right lateral ventricle, which showed intense activity on the day of injection and decreased with time, though persisting partially until 48 h, resulting in an estimated dose of 2.95 cGy/MBq. Radiation doses to other organs besides liver were generally low (Table 2). We recognize, however, that these organ dose estimates are based on limited time-activity data, measured at only 3 time points out to about 48 h after infusion; we therefore also analyzed these data, applying a terminal clearance biologic half-time of 57 h to the actual fits of the organ time-activity data. The 57-h half-time was derived from data for a separate group of patients administered ^{124}I -omburtamab intracranially, for whom whole-body time-activity data were collected out to 6–8 d after administration. The number of time points (4–6) and later time (out to 6 or 8 d) provided confidence in the accuracy of the 57-h clearance half-time. These ^{124}I -omburtamab time-activity data followed a monoexponential (single half-time) function. When this clearance half-time was applied to the fitted functions of a subset of our cohort of ^{131}I -omburtamab patients, for whom the dosimetry is presented in Table 2, these revised absorbed-dose estimates for stomach wall, spleen, and liver were only 20%–30% greater than our original dose estimates. For all other organs, the difference between the original and revised absorbed-dose estimates was less than 5%.

CSF Pharmacokinetics and Dosimetry from CSF

Sample Counts

The CSF clearance was biexponential, with initial half-life averaging less than 1 h followed by a longer second half-life, likely more appropriately representing the rate of clearance of the radio-labeled antibody from the CSF compartment. The mean 25%, 59% (median), and 75% quartile biologic half-lives for ^{124}I clearance are given in Table 3. Most patients exhibited CSF clearance half-lives of less than 24 h, but 3 patients exhibited much longer half-lives (35–46 h), likely because of slower clearance from the Ommaya reservoir and ventricles as noted on the images. Estimates for various age groups in children showed similar values (Table 3).

The estimate for ^{131}I -omburtamab doses as derived from ^{124}I -omburtamab CSF samples was 2.25 ± 0.4 cGy/MBq, whereas that from actual ^{131}I -omburtamab therapy was 1.53 ± 1.44 cGy/MBq (Table 4). Overall doses were highly variable. In 9 patients, the dose estimates ranged between 4.42 and 8.44 cGy/MBq, about 2–4 times higher than the average for all. In another patient, the estimated dose was 10.1 cGy/MBq, based on extrapolation from limited sampling (only at 18 h because of logistical limitations). In 7 of these 10 infusions, a very slow clearance (practically zero in 3 patients) was noted over the initial 8 h; imaging in these patients showed high activity within ventricles and Ommaya up to 48-h imaging.

TABLE 2
Normal Organ-Absorbed Dose and Effective Dose Estimates for ¹²⁴I-Omburtamab Administered Intraventricularly

Site	Mean	SD	Median	Minimum	Maximum
Salivary gland	0.52	0.33	0.44	0.05	1.45
Adrenals	0.41	0.23	0.40	0.06	1.10
Brain	1.13	0.55	1.01	0.20	3.03
Gallbladder wall	0.46	0.24	0.46	0.07	1.13
Lower large intestine wall	0.36	0.22	0.34	0.06	1.02
Small intestine	0.40	0.24	0.38	0.06	1.02
Stomach wall	0.86	0.57	0.71	0.17	2.65
Upper large intestine wall	0.40	0.23	0.39	0.06	1.08
Heart wall	0.39	0.23	0.37	0.06	1.06
Kidneys	0.39	0.22	0.38	0.06	1.05
Liver	1.58	1.04	1.62	0.06	4.22
Lungs	0.36	0.21	0.34	0.05	1.00
Muscle	0.34	0.21	0.31	0.05	0.98
Pancreas	0.44	0.25	0.44	0.07	1.16
Red marrow	0.37	0.27	0.30	0.05	1.21
Osteogenic cells	0.67	0.43	0.59	0.12	1.99
Skin	0.30	0.18	0.27	0.05	0.85
Spleen	0.57	0.32	0.55	0.04	1.16
Thymus	0.35	0.21	0.32	0.05	0.99
Thyroid	0.58	0.74	0.40	0.07	5.29
Urinary bladder wall	0.35	0.21	0.34	0.06	0.98
Total body	0.45	0.27	0.45	0.07	1.22
Effective dose (mSv/MBq)	0.49	0.27	0.47	0.10	1.23
Effective dose equivalent (mSv/MBq)	0.55	0.28	0.53	0.10	1.32

Units are mGy/MBq unless otherwise noted.

Blood Dosimetry Data from Sample Counts

The mean and median radiation dose estimates to the blood from ¹³¹I-mAb-omburtamab and those derived from ¹²⁴I-mAb-omburtamab are 0.051 cGy/MBq (1.87 cGy/mCi) and 0.039 cGy/MBq (1.44 cGy/mCi), respectively (Table 5). The estimates to blood are higher for the therapy than pretherapy tracer samples, a possible consequence

of the slower clearance of the larger administered mass of antibody for the therapeutic administration.

Statistical Analysis

A total of 50 dose estimates of ¹²⁴I/¹³¹I-omburtamab were analyzed. A Wilcoxon signed-rank test comparing the doses from

TABLE 3
PET Imaging and CSF-Derived Biologic Clearance Half-Lives of ¹²⁴I-Omburtamab from CSF

Parameter	Total median	25% Q	50% Q	75% Q	Range	Mean			Median		
						<5 y	5–10 y	>10 y	<5 y	5–10 y	>10 y
¹²⁴ I-omburtamab PET											
Ventricle	8.19	6.61	8.89	9.57	3.6–18.2	9.22	8.62	8.81	8.14	8.3	9.01
Cervical	6.86	6.36	9.08	8.89	3.9–16.9	8.13	9.72	9.54	6.78	6.65	9.7
Thoracic	7.83	6.71	11.01	10.39	5.0–25.0	9.14	12.84	10.82	7.51	7.94	9.87
Lumbar	7.02	6.32	9.84	11.05	4.1–39.6	9.46	9.46	14.91	6.62	6.94	11.47
¹²⁴ I-omburtamab samples	6.3	5.49	10.31	11.63	3.7–46.2	10.15	9.33	9.31	8.41	6.62	5.74

Q = quartile.

Data are in hours and exclude outliers 26 h and 44.4 h in single patient each.

TABLE 4
Radiation Dose Estimates to CSF for ¹³¹I-mAb-Omburtamab

Parameter	Mean	25% quartile	Median	75% quartile	Range
¹²⁴ I-omburtamab PET-derived doses	0.620	0.436	0.523	0.755	0.21–2.948
Ventricle					
Cervical	0.445	0.326	0.387	0.494	0.170–0.711
Thoracic	0.538	0.373	0.442	0.555	0.189–1.978
Lumbar	0.567	0.454	0.552	0.652	0.235–1.051
Whole CSF					
From ¹²⁴ I-omburtamab CSF samples	2.253	0.961	1.443	2.512	0.100–10.243
From ¹³¹ I-omburtamab posttherapy CSF samples	1.534	0.695	1.1	1.841	0.041–8.386

Data are cGy/MBq.

intraventricular ¹²⁴I-omburtamab PET data from ventricles (D_{PET}) versus ¹²⁴I-omburtamab CSF sample data ($D_{samples}$) after intraventricular administration showed a significant difference between the 2 measures in terms of the median difference in distribution ($P < 0.0001$). The Pearson correlation coefficient was 0.00655 ($P = 0.96$), indicating no correlation between the 2 values (Fig. 3A). In most patients, sample-based estimates of activity concentrations were higher than the PET-based estimates, and in only 3 patients were the PET-based estimates greater than the sample-based estimate. This result is further illustrated by the Bland–Altman analysis (Fig. 3B). In the Bland–Altman plot, each point represents the difference ($D_{PET} - D_{samples}$) on the y-axis versus the average ($(D_{PET} + D_{samples})/2$) on the x-axis for an individual patient. The Bland–Altman plot shows a systematic increase in the difference between the PET and sample dosimetry estimates with increasing magnitude of the averaged values. This bias is likely a consequence of the higher CSF sample values' being associated with slower mixing with the CSF compartment.

For CSF sample data from pretreatment ¹²⁴I-omburtamab and ¹³¹I-omburtamab posttreatment samples, the Wilcoxon signed-rank test showed significant differences ($P = 0.013$) and the Pearson correlation coefficient was 0.084 with a P value of 0.52, indicating no correlation (Fig. 3C). However, as expected, the paired samples were almost equally distributed about the line of identity, suggesting no systematic difference between the 2 sample-based dose estimates.

DISCUSSION

Intraventricular infusions of therapeutic agents allow for treating compartmentalized disease while limiting systemic toxicity. To optimize therapeutic outcome, understanding the kinetics and dosimetry of the therapeutic agent is essential. Multiple CSF sampling either

directly via lumbar puncture or an access catheter such as the Ommaya system allows for direct measurement of the radioactivity but is invasive, with a risk of infection, and can be limiting in children. We evaluated the feasibility and utility of ¹²⁴I-omburtamab PET imaging for estimating the projected dose for ¹³¹I-omburtamab therapy administered intraventricularly.

With ¹²⁴I/¹³¹I-omburtamab injected directly into the CSF compartment, there was higher activity concentrations within the CSF space and low activity elsewhere during the imaging times; the image quality and target-to-background contrast of ¹²⁴I-omburtamab were excellent. The antibody clearance was slow, as visualized by the sequential PET images, allowing for longer duration of radiation exposure to the CSF space and leptomeninges. The dose-limiting toxicity from intravenous administration of radiolabeled antibody therapy was from bone marrow toxicity (typically a 200-cGy limit). The relative CSF-to-blood dose ratios were extremely high, ranging between 10-fold for PET-based values to 30–45 for CSF sample-based estimates. Our data suggest that an administered activity of approximately 4,000 MBq of ¹³¹I-omburtamab could be administered before exceeding a blood dose of 200 cGy. Therefore, even at treatment doses of 1,850–2,960 MBq (50–80 mCi) given intraventricularly, the blood dose was well below the generally accepted safe limit; thus, no significant marrow toxicity was generally seen.

Our data indicate a wide variation in doses estimated from CSF samples (Table 4). This variation is likely due to the retrieval technique of CSF samples from the same Ommaya port as that into which the radiolabeled antibody was injected, where pooling of activity in the reservoir is present, as noted in imaging. In contrast, far less variation was noted with PET imaging–based estimates, for which the activity in the Ommaya that generates high counts can be and was excluded from the PET VOI ventricle estimates. This also explains the consistently lower PET-based estimates than CSF sample–derived estimates. The dose estimates to the different CSF subregions was more consistent. Only in a single patient did we observe substantial activity retained in the lateral ventricle on PET images; this was attributed to disease and treatment changes. In this patient, the PET estimate of CSF activity concentration was higher than that measured in CSF samples; this patient exhibited prominent ventricular retention, likely related to disease.

We found no significant statistical correlation between CSF sample–based and PET-based estimates. Overall, the radiation dose estimates from ¹²⁴I CSF sample data was much greater than that from PET data: 2.36 versus 0.63 cGy/MBq, a ratio of 3.74.

TABLE 5
Blood Dosimetry Estimates for ¹³¹I-mAb-Omburtamab Derived from Pretherapy ¹²⁴I-Omburtamab Administration and Actual ¹³¹I-Omburtamab Therapy

Omburtamab blood sample	Mean dose (cGy/MBq)	Median dose (cGy/MBq)	Dose range (cGy/MBq)
¹²⁴ I	0.051	0.039	0.0035–0.244
¹³¹ I	0.068	0.069	0.0032–0.158

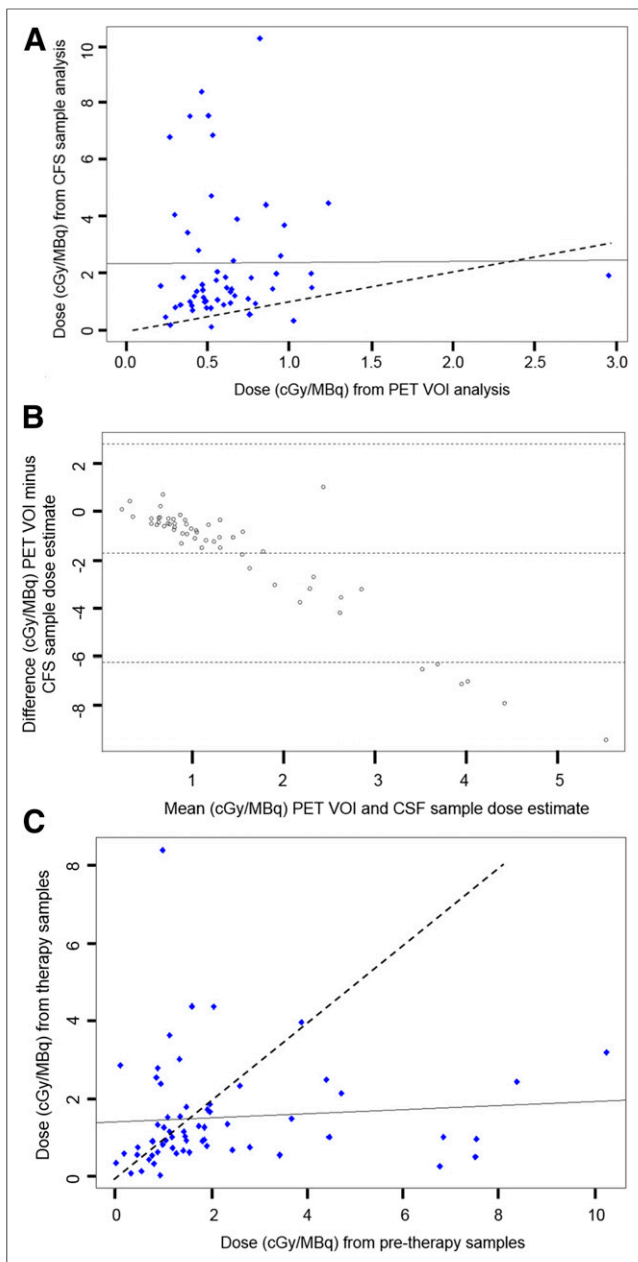


FIGURE 3. CSF dose estimates for ^{124}I -omburtamab: ^{124}I -omburtamab PET estimates vs. actual ^{124}I -omburtamab CSF samples. (A) Scatterplot showing estimated radiation doses for ^{131}I -omburtamab in units of cGy/MBq. x-axis shows dose values estimated from ^{124}I -8H9 PET region-of-interest data vs. doses estimated from ^{124}I -8H9 CSF sample counts on y-axis. Pearson correlation coefficient was calculated to show correlation between PET region of interest vs. sample count data. This coefficient is 0.00655 with P value of 0.96, indicating no correlation. Solid and dashed lines represent lines of correlation and identity, respectively. (B) Bland–Altman plot showing mean difference between PET region-of-interest dose and CSF sample-based dose estimates on y-axis vs. average of 2 dose estimates on x-axis; 95% confidence intervals for mean difference was determined using R package “Bland–Altman Leh.” (C) Scatterplot comparing radiation doses (cGy/MBq) from posttherapy ^{131}I -omburtamab samples (y-axis) vs. pretherapy ^{124}I -omburtamab samples (x-axis). Pearson coefficient is 0.084 with P value of 0.52, indicating no correlation. Solid and dashed lines represent lines of correlation and identity, respectively.

Although in a small group of patients there was agreement between the PET and sample-based dose estimates, most showed greater variation. Therefore, dosimetry estimates based on Ommaya samples were found to be less reliable than image-based methods. This is further underscored by the statistical analysis comparing the pretherapy ^{124}I -omburtamab CSF sample data and the posttherapy ^{131}I -omburtamab CSF data, for which no significant correlation was found (Fig. 3C). Additionally, whereas differences in the clearance time and dosimetry noted for pretherapy versus posttherapy estimates could in part reflect the differing mass amounts of antibody administered, the lack of significant bias does not support this possibility.

The limitations of this study include the comparison of CSF sampling data, which is affected by the technique of sampling (i.e., from the same port into which the radiolabeled antibody was injected). This is a limitation, especially in children, for whom a separate CSF draw from lumbar puncture at each time point is impractical. Noninvasive imaging methods are therefore preferred. A general practical limitation to ^{124}I imaging is the expense. An alternative approach may be to use dose estimates based on serial γ -camera scans and SPECT imaging with ^{131}I -omburtamab, though quantitation of single-photon activity remains less reliable in routine clinical practice than that of positron-emitting radionuclides.

CONCLUSION

^{124}I -omburtamab PET imaging is a noninvasive method to obtain dosimetry estimates in patients undergoing intraventricular therapy with ^{131}I -omburtamab. ^{124}I -omburtamab PET imaging dosimetry estimation shows less variation than estimates by CSF sampling.

DISCLOSURE

This research was funded in part through the NIH/NCI Cancer Center Support Grant P30 CA008748. Neeta Pandit-Taskar has served as a consultant to Y-mAbs Therapeutics, Inc., served on an advisory board of and received honoraria from Actinium Pharmaceuticals, and served on the advisory board of Progenics. She has received honoraria from MedImmune/AstraZeneca. Milan Grkovski and Edward Fung received support from Y-mAbs Therapeutics, Inc. Serge Lyashchenko reports personal fees from Y-mAbs Therapeutics, Inc., outside the submitted work. Jorge Carrasquillo has served as a consultant for Y-mAbs Therapeutics, Inc., and Bayer and has received research funding from Genentech, Inc., Regeneron Pharmaceuticals, Inc., and Gilead Sciences, Inc. With regard to this publication, Jason Lewis’s laboratory has received research support from Y-mAbs, Inc. Steven Larson reports receiving commercial research grants from Genentech, Inc., WILEX AG, Telix Pharmaceuticals Limited, and Regeneron Pharmaceuticals, Inc.; holding ownership interest/equity in Voreyda Theranostics Inc. and Elucida Oncology Inc.; and holding stock in ImaginAb, Inc. He is the inventor and owner of issued patents both currently unlicensed and licensed by MSK to Samus Therapeutics, Inc., Elucida Oncology, Inc., and Y-mAbs Therapeutics, Inc. He is serving or has served as a consultant to Cynvec LLC, Eli Lilly & Co., Prescient Therapeutics Limited, Advanced Innovative Partners, LLC, Gerson Lehrman Group, Progenics Pharmaceuticals, Inc., and Janssen Pharmaceuticals, Inc. Nai-Kong Cheung reports receiving commercial research grants from Y-mAbs Therapeutics, Inc., in 2015 and Abpro-Labs, Inc., in 2017; holding ownership interest/equity in Y-mAbs Therapeutics and in Abpro-Labs; and owning stock options in Eureka Therapeutics, Inc. He is the

inventor and owner of issued patents licensed by MSK to Y-mAbs Therapeutics, Biotec Pharmacon, and Abpro Labs. He is a scientific advisory board member of Abpro Labs and Eureka Therapeutics and is named as an inventor on several patent applications related to GPA33 filed by MSK. No other potential conflict of interest relevant to this article was reported.

KEY POINTS

QUESTION: Does PET imaging of intrathecally administered ^{124}I -omburtamab add value to the dosimetric estimates for ^{131}I radioimmunotherapy of leptomeningeal disease?

PERTINENT FINDINGS: PET imaging provides more robust kinetic and biodistribution data than CSF sampling and overcomes artifact-related errors associated with CSF sampling.

IMPLICATIONS FOR PATIENT CARE: PET imaging complements CSF analysis and can allow for more optimal estimates through combined analysis and imaging assessment.

REFERENCES

1. Kramer K, Kushner B, Heller G, Cheung NK. Neuroblastoma metastatic to the central nervous system: the Memorial Sloan Kettering Cancer Center experience and a literature review. *Cancer*. 2001;91:1510–1519.
2. Kramer K, Kushner BH, Modak S, et al. Compartmental intrathecal radioimmunotherapy: results for treatment for metastatic CNS neuroblastoma. *J Neurooncol*. 2010;97:409–418.
3. Akabani G, Reardon DA, Coleman RE, et al. Dosimetry and radiographic analysis of ^{131}I -labeled anti-tenascin 81C6 murine monoclonal antibody in newly diagnosed patients with malignant gliomas: a phase II study. *J Nucl Med*. 2005;46:1042–1051.
4. Bigner DD, Brown MT, Friedman AH, et al. Iodine-131-labeled antitenascin monoclonal antibody 81C6 treatment of patients with recurrent malignant gliomas: phase I trial results. *J Clin Oncol*. 1998;16:2202–2212.
5. Cheung NK, Kushner BH, Cheung IY, et al. Anti-G(D2) antibody treatment of minimal residual stage 4 neuroblastoma diagnosed at more than 1 year of age. *J Clin Oncol*. 1998;16:3053–3060.
6. Kramer K, Cheung NK, Humm JL, et al. Targeted radioimmunotherapy for leptomeningeal cancer using ^{131}I -3F8. *Med Pediatr Oncol*. 2000;35:716–718.
7. Kramer K, Humm JL, Souweidane MM, et al. Phase I study of targeted radioimmunotherapy for leptomeningeal cancers using intra-Ommaya ^{131}I -3F8. *J Clin Oncol*. 2007;25:5465–5470.
8. Modak S, Kramer K, Gultekin SH, Guo HF, Cheung NK. Monoclonal antibody 8H9 targets a novel cell surface antigen expressed by a wide spectrum of human solid tumors. *Cancer Res*. 2001;61:4048–4054.
9. Xu H, Cheung IY, Guo HF, Cheung NK. MicroRNA miR-29 modulates expression of immunoinhibitory molecule B7-H3: potential implications for immune-based therapy of human solid tumors. *Cancer Res*. 2009;69:6275–6281.
10. Stabin MG, Sparks RB, Crowe E. OLINDA/EXM: the second-generation personal computer software for internal dose assessment in nuclear medicine. *J Nucl Med*. 2005;46:1023–1027.
11. Morishita Y, Naito M, Hymanson H, Miyazaki M, Wu G, Wang JC. The relationship between the cervical spinal canal diameter and the pathological changes in the cervical spine. *Eur Spine J*. 2009;18:877–883.
12. Lee HJ, Kim JT, Shin MH, Choi DY, Hong JT. Quantification of pediatric cervical spine growth at the cranio-vertebral junction. *J Korean Neurosurg Soc*. 2015;57:276–282.
13. Eckerman KF, Endo A. *MIRD Radionuclide Data and Decay Schemes*. 2nd ed. Reston, VA: Society of Nuclear Medicine and Molecular Imaging; 2008.